ESCAPES AND RECURRENCE IN A SIMPLE HAMILTONIAN SYSTEM

G. CONTOPOULOS and K. EFSTATHIOU
Academy of Athens, Research Center for Astronomy, 14 Anagnostopoulou Str., GR-10673, Athens, Greece, e-mail: gcontop@cc.uoa.gr

(Received: 28 March 2003; revised: 21 July 2003; accepted: 18 August 2003)

Abstract. Many physical systems can be modeled as scattering problems. For example, the motions of stars escaping from a galaxy can be described using a potential with two or more escape routes. Each escape route is crossed by an unstable Lyapunov orbit. The region between the two Lyapunov orbits is where the particle interacts with the system. We study a simple dynamical system with escapes using a suitably selected surface of section. The surface of section is partitioned in different escape regions which are defined by the intersections of the asymptotic manifolds of the Lyapunov orbits with the surface of section. The asymptotic curves of the other unstable periodic orbits form spirals around various escape regions. These manifolds, together with the manifolds of the Lyapunov orbits, govern the transport between different parts of the phase space. We study in detail the form of the asymptotic manifolds of a central unstable periodic orbit, the form of the escape regions and the infinite spirals of the asymptotic manifolds around the escape regions. We compute the escape rate for different values of the energy. In particular, we give the percentage of orbits that escape after a finite number of iterations. In a system with escapes one cannot define a Poincaré recurrence time, because the available phase space is infinite. However, for certain domains inside the lobes of the asymptotic manifolds there is a finite 'minimum recurrence time'. We find the minimum recurrence time as a function of the energy.

Key words: asymptotic manifolds, escapes, Hamiltonian dynamics, Poincaré recurrence

1. Introduction

The problem of escapes from a dynamical system has been discussed by many authors. The most recent aspect of this problem is the subject of chaotic escapes, or chaotic scattering (Bleher et al., 1988; Eckhardt, 1988; Ott and Tél, 1993). Particular cases refer to the encounters of two satellites around a planet (Petit and Hénon, 1986), the interactions of particles in the rings of Saturn (Hénon, 1989),the scattering of particles in a magnetic dipole (Jung and Scholz, 1988), the scattering of photons or particles by two fixed black holes (Contopoulos, 1990b, 1991), the escapes of stars from a galaxy (Contopoulos, 1990a; Contopoulos and Kaufmann, 1992) and the escapes in the restricted three-body problem (Benet et al., 1997, 1998).

Celestial Mechanics and Dynamical Astronomy **88:** 163–183, 2004.

There are indications that escapes from simple galactic models follow a universal pattern (Siopis et al., 1997; Kandrup et al., 1999). In particular the escape rate p_∞ in strongly chaotic systems seems to follow a law $p_\infty \sim (\epsilon - \epsilon_{\rm crit})^a$, where ϵ is the perturbation, $\epsilon_{\rm crit}$ is a critical perturbation, and a is a universal constant, close to $a = 0.5$.

Of special interest is the study of the various domains of escape. Such domains in general form infinite spirals around some limiting asymptotic curves (Contopoulos, 1990a; Contopoulos and Kaufmann, 1992; Contopoulos and Polymilis, 1993; Henrard and Navarro, 2001). In the present paper we study in more detail the escape domains in a simple dynamical system that has been used as a model of the central region of a galaxy.

In Section 2 we find the escape domains and show that they form infinite spirals around the asymptotic manifolds of some particular unstable periodic orbits called Lyapunov orbits. We find the intersections of the escape domains in the forward and the backward time directions. In Section 3 we study the rate of escapes of the orbits. Then, in Section 4, we study the asymptotic curves of the central unstable periodic orbit. The forms of these asymptotic curves are related to the shape of the escape domains. In Section 5 we find the minimum Poincaré recurrence time for various energies. For large energies the minimum recurrence time decreases and reaches one iteration. In Section 6 we consider the resonant case 1:1 and we describe the similarities and the differences between this and the previous case. Finally, in Section 7 we write our conclusions.

2. Escapes

We consider a Hamiltonian

$$H(x, y, p_x, p_y) = \tfrac{1}{2}(p_x^2 + p_y^2 + Ax^2 + By^2) - \epsilon xy^2 = h, \tag{1}$$

where $A = \omega_1^2 = 1.6$, $B = \omega_2^2 = 0.9$ and $\epsilon = 0.08$. This is a higher order resonance case (4:3), but in most respects it represents also the nonresonant cases.

This Hamiltonian is symmetric with respect to the transformation $y \to -y$. When the isoenergetic surface is compact, that is, for values of the energy smaller than the escape energy, almost all orbits intersect the surface $y = 0$ transversally because of this symmetry. Thus, the surface $y = 0$ is a Poincaré surface of section. The only exception is the x-axis family ($y = 0$, $p_y = 0$) that stays on the surface $y = 0$. This orbit is the boundary of the phase space on the surface of section $y = 0$. The areas on the Poincaré surface of section are preserved.

However, when we have escapes (Figure 1), the surface $y = 0$ is not a Poincaré surface of section. Some orbits may not intersect this surface, or intersect it only a finite number of times and then escape to infinity. One consequence of this fact is that the areas may not be preserved on this surface. The measure m' of the image of an area of measure m on the surface $y = 0$ is in general smaller than

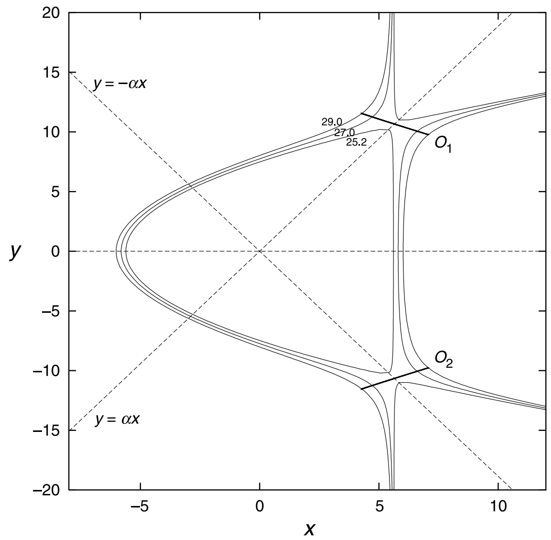

Figure 1. Equipotentials for various values of the energy h. The Lyapunov orbits for $h = 29$ are O_1 and O_2. The main axes are x and y. The straight lines are $y = \pm\alpha x$, where $\alpha = (2A/B)^{1/2}$. These lines are periodic orbits for energies smaller than h_{esc}.

m. Nevertheless, the study of the intersections of the orbits by the surface $y = 0$ is of interest, since it allows us to understand a large part of the dynamics. The surface $y = 0$ is then a 'local surface of section' (Birkhoff, 1927).

The escape energy in the case (1) is equal to

$$h_{\mathrm{esc}} = \frac{AB^2}{8\epsilon^2}. \tag{2}$$

In the present case $h_{\mathrm{esc}} = 25.31$.

When the value of the energy h becomes larger than the escape energy h_{esc}, the equipotentials are open and extend to infinity. Then two unstable periodic orbits, called Lyapunov orbits, are formed, crossing the openings of the equipotentials (Figure 1). We denote the Lyapunov orbits by O_1 and O_2. Lyapunov orbits are important for the escapes from the system, since if an orbit intersects any one of these orbits outwards it escapes to infinity without any further intersections with the surface of section (Churchill et al., 1975).

For a fixed value of the energy $h = 29$, the initial conditions of orbits on the surface (x, p_x) with $y = 0$ and $p_y > 0$, that escape immediately or after one intersection with the surface $y = 0$ are denoted by different shades of gray in Figure 2(a). The elliptical boundary surrounding Figure 2(a) represents the curve $y = p_y = 0$, therefore it is given by the equation

$$p_x^2 + Ax^2 = 2h. \tag{3}$$

No motion is possible outside this curve.

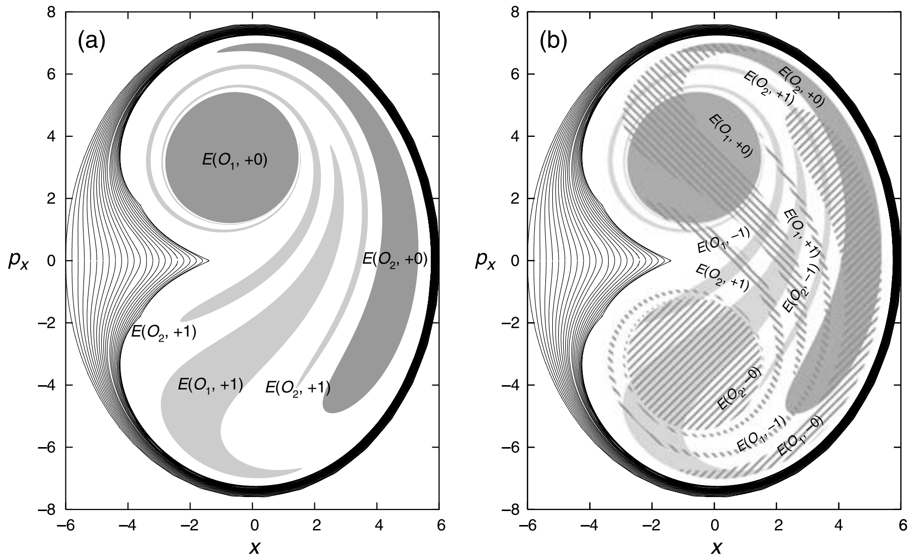

Figure 2. The escape regions $E(O_i, +0)$ and $E(O_i, +1)$ $(i = 1, 2)$ in the space (x, p_x) for $y = 0$, $p_y > 0$ and $h = 29$ (gray). (b) The escape regions of (a) plus the symmetric escape regions $E(O_i, -0)$ and $E(O_i, -1)$ (hached). Near the boundary of the figures we have drawn several invariant curves that surround the escape regions (some of them are so close that they form a black ribbon). Most of the points of the white regions, between the escape regions above, escape after longer times.

The regions $E(O_i + n)$, $i = 1, 2$ of Figure 2(a) represent regions of initial conditions of orbits that escape to infinity in the forward time direction after intersecting n times the surface $y = 0$, besides the initial point. By $E(O_i, +0)$ we denote the regions of orbits that escape to infinity in the forward time direction without any further intersection with the surface $y = 0$. Notice here that, by definition, the intersections of an orbit by the (local) surface of section $y = 0$ are considered only when $p_y > 0$.

Furthermore, we distinguish the escape regions by the Lyapunov orbit through which the orbits escape. We denote by $E(O_1, +n)$ the initial conditions of orbits that escape to infinity through O_1 and by $E(O_2, +n)$ the initial conditions of orbits that escape to infinity through O_2. In a similar way we consider the regions $E(O_i, -n)$ that escape in the backward time direction after n intersections besides the initial point. In Figure 2(b) we give both regions $E(O_{1,2}, \pm 0)$ and $E(O_{1,2}, \pm 1)$. We note that the regions $E(O_2, -n)$ and $E(O_2, +n)$ are symmetric to the regions $E(O_1, +n)$ and $E(O_1, -n)$, respectively.

The boundaries of the regions $E(O_1, +0)$ and $E(O_1, -0)$ are the first intersections of the stable and unstable manifold, respectively, of the Lyapunov orbit O_1 with the surface of section $y = 0$. Similarly, the boundaries of the regions $E(O_2, +0)$ and $E(O_2, -0)$ are the first intersections of the stable and unstable manifolds of O_2 with the surface of section. Furthermore, we have checked that the area of $E(O_1, +0)$ is equal to the area of $E(O_2, +0)$, as it should be expected, because of the symmetry of the system (1).

In Figure 2(a) we see also the regions $E(O_{1,2}, +1)$. The region $E(O_1, +1)$ is a single connected piece. The region $E(O_2, +1)$, on the other hand, is composed of two pieces that make infinite spiral rotations around the region $E(O_1, +0)$. We have checked that the area of $E(O_1, +1)$ is equal to the area of $E(O_1, +0)$, while the sum of the areas of the two spiraling regions $E(O_2, +1)$ is smaller than the area of $E(O_2, +0)$.

We can understand this difference as follows. The region $E(O_1, +0)$ after one iteration in the backward time direction is mapped into the region $E(O_1, +1)$. No orbits from the region $E(O_1, +0)$ escape between the times $t = 0$ and $t = -1$ because the region $E(O_1, +0)$ does not intersect either one of the regions $E(O_{1,2}, -0)$ (Figure 2(b)). Therefore, the orbits starting in the region $E(O_1, +0)$ reach the region $E(O_1, +1)$ and as a consequence the areas of these regions are equal. However, if we start orbits in the region $E(O_2, +0)$ backward in time, only part of them intersect again the plane (x, p_x) at $t = -1$ inside the regions $E(O_2, +1)$. These orbits belong to the two parts of $E(O_2, +0)$ outside the region $E(O_1, -0)$. But the orbits starting at the intersection of $E(O_1, -0)$ and $E(O_2, +0)$, escape immediately, backwards in time, before $t = -1$ and are not mapped to $E(O_2, +1)$. As a consequence the total area of the regions $E(O_2, +1)$ is smaller than the area of $E(O_2, +0)$ by an amount equal to the area of $E(O_1, -0) \cap E(O_2, +0)$.

Another consequence of the intersection of $E(O_1, -0)$ with $E(O_2, +0)$ is the existence of infinite spiral rotations of the regions $E(O_2, +1)$ around $E(O_1, +0)$. This can be explained as follows. The boundary of $E(O_1, -0)$ is on the unstable manifold of the Lyapunov orbit O_1. Orbits inside this boundary escape for negative times directly from O_1 (without any further intersection with the plane (x, p_x)). On the other hand, orbits close but outside $E(O_1, -0)$ approach O_1 for negative times, but do not reach O_1. Instead, they deviate later (for larger $-t$) from O_1, staying close to the stable manifold of O_1, and reach the plane (x, p_x) close to the boundary of $E(O_1, +0)$ (which is the first intersection of the stable manifold of O_1 with the surface of section) but outside it. If the initial point is very close to the boundary of $E(O_1, -0)$, the next intersection with the plane (x, p_x) after approaching O_1 (for negative t always), is very close to $E(O_1, +0)$. Thus, the parts of $E(O_2, +0)$ very close but outside $E(O_1, -0)$, give images on the (x, p_x) plane that approach arbitarily closely the boundary of $E(O_1, +0)$. Moreover, as the initial condition on $E(O_2, +0)$ approaches $E(O_1, -0)$ the time the orbit needs to intersect the plane (x, p_x) goes to infinity and so does the number of revolutions around the stable manifold of O_1 and around $E(O_1, +0)$. Because of this the images of the points of $E(O_2, +0)$ close to the boundary of $E(O_1, -0)$ form spirals around $E(O_1, +0)$.

For a larger value of the energy h the regions $E(O_1, +0)$ and $E(O_1, -0)$ intersect (the situation for $h = 40$ is depicted in Figure 3) and then the areas of the corresponding regions $E(O_1, +1)$ and $E(O_1, -1)$ are smaller. We notice that in this case the regions of escape $E(O_2, +0)$ and $E(O_1, -0)$ form infinite rotations

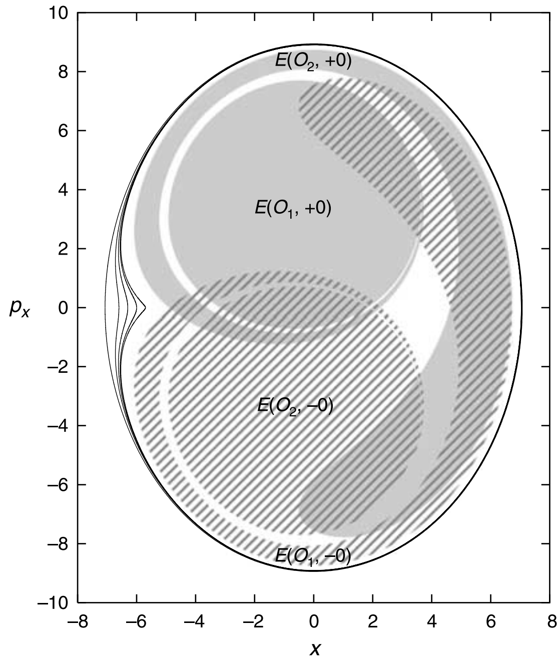

Figure 3. The escape regions $E(O_{1,2}, \pm 0)$ in the space (x, p_x) for $h = 40$. The region $E(O_1, +0)$ intersects the axis $p_x = 0$, therefore it intersects also the symmetric region $E(O_2, -0)$.

around the regions $E(O_1, +0)$ and $E(O_2, -0)$, respectively. Similar considerations apply to regions that escape after two or more intersections with the (x, p_x) plane. These are represented by thinner filaments, and their areas are smaller, for the same reason as above.

Finally, in Figure 2(a) and (b) we see an outer ring of orbits that never escape. These are orbits that form smooth invariant curves, surrounding the regions of escape. These orbits remain close to the axis $y = 0$ because the values of p_y along them are small (the outer boundary represents the orbit $y = p_y = 0$, i.e. the x-axis). Between these invariant curves there are small higher order islands of stability and very small chaotic zones between them. (These are not conspicuous in Figure 2(a) and (b).)

As the energy h decreases the whole escaping area decreases. If h becomes smaller than $h_{\rm esc}$ there are no escapes at all, but a large part of the surface of section (x, p_x) is chaotic. This is seen in Figure 4, where we mark the chaotic and ordered domains for $h = 25.2$, a value smaller than the escape energy $h_{\rm esc} = 25.31$. In this case the chaotic domain contains some islands of stability. Two islands 2:1 belong to the same orbit that makes two oscillations in the x-direction while making one oscillation in the y-direction. Two more islands 2:1 correspond to orbits symmetric to the above (white regions in Figure 4). There are also two islands corresponding to resonant 1:1 orbits. One of them is marked in Figure 4, while the other is a white region symmetric to the first with respect to the axis $p_x = 0$. When h goes just beyond $h_{\rm esc}$ it seems that almost all chaotic orbits escape to infinity after a

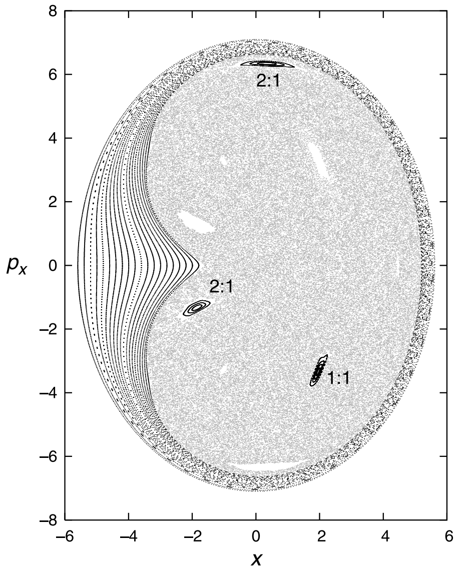

Figure 4. Invariant curves and a large chaotic domain on the surface of section (x, p_x) for $h = 25.2$ ($< h_{\rm esc} = 25.31$). In some islands inside the chaotic domain we have drawn a few invariant curves.

number of intersections with the plane (x, p_x). But, as we will see below, the time of escape is large if h is only slightly above $h_{\rm esc}$. On the other hand, when h becomes larger the escapes are faster and the escaping domains become larger. At the same time the islands of stability of the chaotic domain (Figure 4) become smaller and beyond some critical value $h = h_{\rm crit}$ they practically disappear. Thus most of the orbits starting in the central domain of Figure 2(b) escape.

The main orbits in the escape domain that do not escape are the periodic orbits. The stable periodic orbits are surrounded by islands of stability, but these are very small, especially for large h. On the other hand the unstable periodic orbits are accompanied by stable and unstable asymptotic curves. Orbits starting on a stable asymptotic curve never escape as $t \to +\infty$, and orbits starting on an unstable asymptotic curve never escape as $t \to -\infty$. Furthermore, the intersections of the stable and the unstable manifolds of unstable periodic orbits (homoclinic or heteroclinic points) do not lead to orbits that escape for $t \to \pm\infty$. The measure of these asymptotic orbits is zero. Nevertheless, the structure of the asymptotic curves is of special interest, because they limit various regions of escaping orbits. We will study the asymptotic curves in detail in Section 4.

3. Rate of Escapes

We studied the rate at which the orbits escape to infinity for energies slightly above the escape energy $h_{\rm esc}$. For each value of the energy we considered a grid of initial conditions on the (x, p_x) plane and determined the escape time for each orbit.

For this purpose we iterated each orbit for at most $n = 200$ crossings with the surface of section. If after that time (number of crossings) the orbit had not crossed the Lyapunov orbits we marked it as non-escaping. For every energy we considered a grid of initial conditions where the distance between adjacent nodes in the grid was 5×10^{-3}.

In Figure 5(a) we show the distribution of the escape times for energies from $h = 25.4$ to $h = 28.5$. Specifically, for each value of the energy, we have plotted the quantity $\mathrm{d}N_n/(N_0 - N_{\mathrm{non}})$, where $\mathrm{d}N_n$ denotes the number of orbits that escape between the n and $n+1$ iterations, N_0 is the total number of orbits and N_{non} is the number of non-escaping orbits. We notice that for $h = 25.4$ (very close to the escape energy) there is a sharp initial reduction of the escape rate and then the

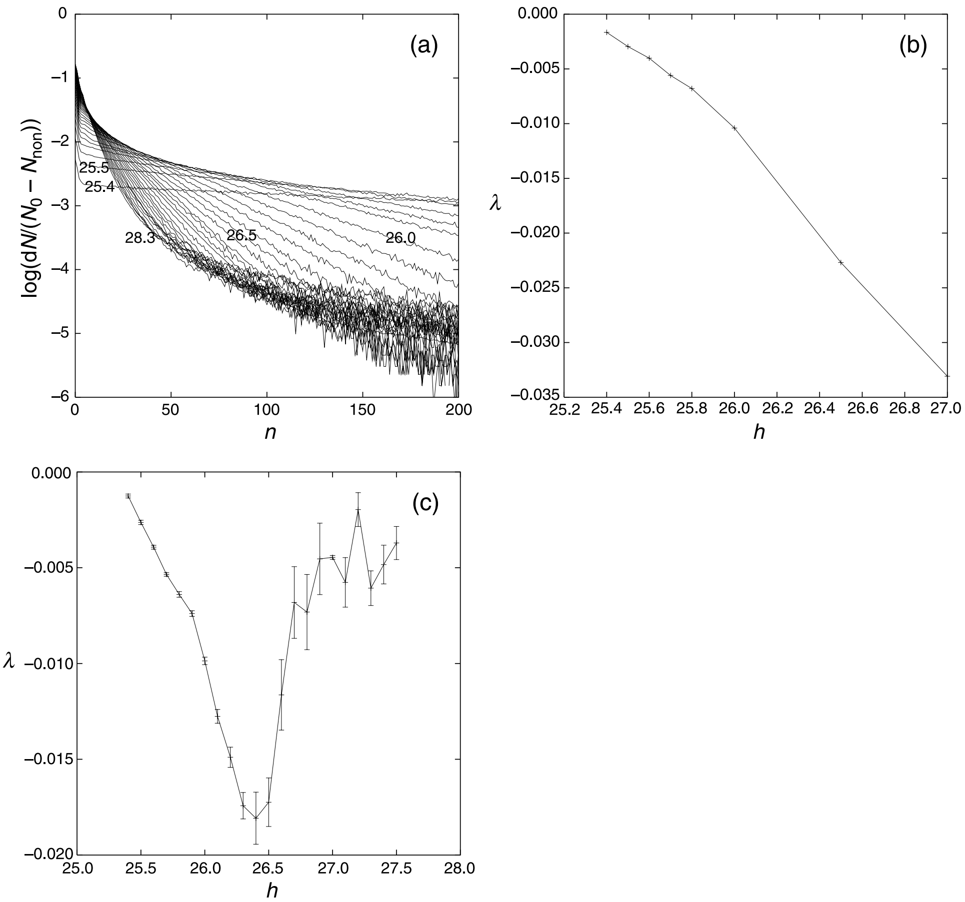

Figure 5. (a) Curves giving the escape rate for several energies. The curves cover the range of energies from $h = 25.4$ to $h = 28.3$ with a step $\mathrm{d}h = 0.1$. We have marked the values of the energy in some curves. (b) The average inclination of these curves around $n = 50$, as a function of the energy h. (c) The inclinations around $n = 180$.

escape rate becomes almost constant. We note here that the escape rate cannot be exactly constant since that would require an infinite volume in phase space.

For larger energies the initial reduction becomes slightly less abrupt (Figure 5(a)) but after a larger time (larger n) the inclination of the curve becomes absolutely smaller. In general these curves are made up of three parts with different inclinations. Namely after the first abrupt reduction there is a large part, with a smaller (absolutely) inclination. For larger n the inclination changes again and becomes even smaller (absolutely).

The almost constant inclination, λ, of the curves becomes more negative with increasing energy. For $n = 50$ the inclination λ is given approximately by a formula

$$\lambda = -0.02(h - h_{\text{esc}}) + 0.0017 \tag{4}$$

as shown in Figure 5(b).

For larger times n (e.g. $n = 180$, Figure 5(c)) the inclination becomes first absolutely larger, as h increases, but for even larger energies ($h > 26.4$) it becomes absolutely smaller. Thus, the inclination for energies beyond $h = 27$ is absolutely smaller than for energies near $h = 26.4$ (Figure 5(c)).

Finally, in Figure 5(a) we notice that the almost constant value of the inclination lasts longer (i.e. up to larger n) as the energy h decreases.

4. Asymptotic Curves

The most important periodic orbit is the 'central' periodic orbit O which tends to one point at the center ($x = y = 0$) as h goes to 0. This is stable for small h, but unstable for $h > h_0 = 22.16$.

The structure of the asymptotic curves from the central periodic orbit O for h smaller than the escape energy h_{esc} is well known (Contopoulos and Polymilis, 1993; some cases with $h > h_{\text{esc}}$ have been also explored). Here we compare two cases with h larger than h_{esc}, namely $h = 27$ (Figure 6) and $h = 29$ (Figure 8).

We first recall here the terminology used by Contopoulos and Polymilis (1993). The unstable asymptotic curve U intersects the stable asymptotic curve S at the point P_0, at roughly equal distances from O along U and S (Figure 6). The region between the arcs OP_0 along U and S is called a resonance. The curve U intersects S outwards from the resonance region at the points $P_0, P_1, P_2, \ldots$ and inwards at the points $P_1', P_2', P_3', \ldots$. The arcs OP_0, OP_1, OP_2 along S are reduced by a factor approximately equal to λ where $\lambda > 1$ is the larger eigenvalue of the orbit O. The same is true for the intervals OP_1', OP_2', etc. Similarly the curve S intersects U outwards at the points $P_0, P_{-1}, \ldots$ and inwards at the points $P_0', \ldots$. The arcs P_0P_1' along U and S form an outer lobe U_1', the arcs $P_1'P_1$ form an inner lobe U_1 and in the same way the arcs P_1P_2' form an outer lobe U_2', the arcs $P_2'P_2$ form the inner lobe U_2, etc. Similarly we have the outer lobe P_0P_0' and the inner lobe $P_0'P_{-1}$ that are called S_0 ($\equiv U_0$) and S_0' ($\equiv U_0'$) lobes respectively (Figure 6).

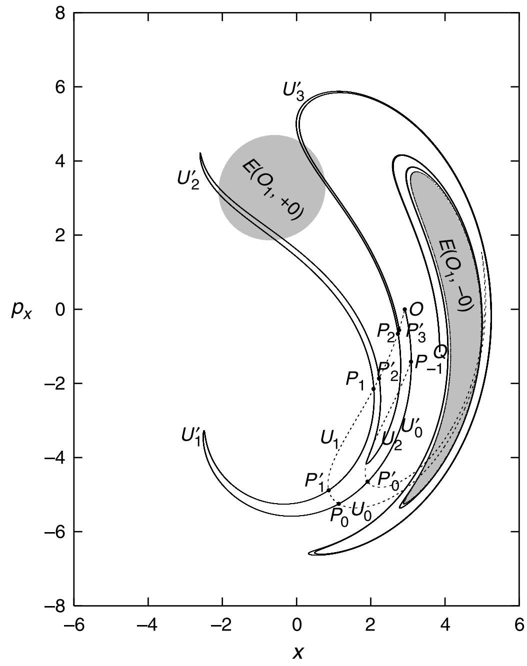

Figure 6. Asymptotic curves from the unstable periodic orbit O: U (solid line up to P_3') and S (dotted line up to P_{-1}) in the case $h = 27$. These curves form the lobes U_0', U_0, U_1', U_1, U_2', U_2 and U_3'. The escape regions $E(O_1, -0)$ and $E(O_1, +0)$ are gray.

In the case $h = 27$ the lobe U_2' leads to escapes (Figure 6). Therefore, the lobe U_3' consists only of the images of non-escaping points of U_2'. The boundary of the lobe U_3' starts at P_2 and makes infinite clockwise rotations around a limiting curve on the right of the figure, namely the boundary of the region $E(O_1, -0)$. Then another arc of U_3' returns with infinite counterclockwise rotations and reaches the point Q (between O and $E(O_1, -0)$). This arc continues by returning in a clockwise way along almost exactly the same curve from Q to the limiting curve of $E(O_1, -0)$. Finally another arc starts again at the limiting curve of $E(O_1, -0)$, very close to the original arc of U_3', but in a counterclockwise way, terminating the boundary of the lobe P_3', at the point P_3', very close to P_2 (Figure 6).

The form of the curve U_3' is rather strange. It is composed of three arcs that make infinite rotations around $E(O_1, -0)$ (the central one makes twice infinite rotations around $E(O_1, -0)$). In order to verify that such a form is to be expected we examined more carefully the lobe U_2' of Figure 6. We noticed that this lobe intersects the escape region $E(O_1, +0)$. The four points of intersection after one iteration correspond to the four infinite rotations of U_3' around the escape region $E(O_1, -0)$. The arc of the curve U_2', beyond the region $E(O_1, +0)$, after one iteration forms the central arc of U_3', that reaches the point Q after infinite counterclockwise rotations from the boundary of the region $E(O_1, -0)$ and then returns from Q to $E(O_1, -0)$ after infinite clockwise rotations.

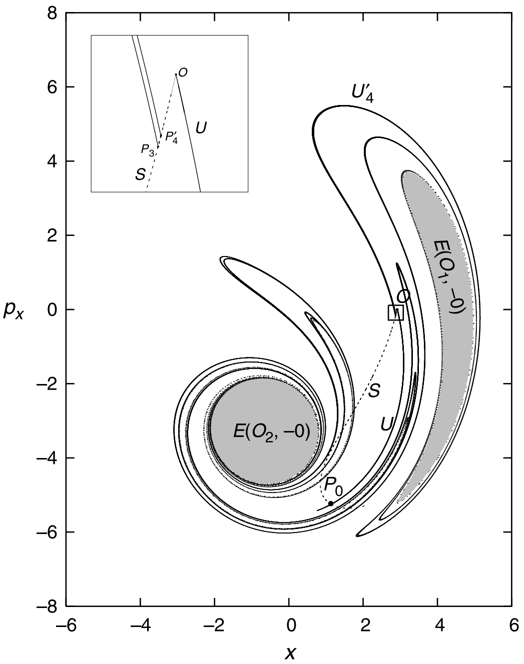

Figure 7. The lobe U'_4 in the case $h = 27$. In the inset we show the beginning of the lobe at P_3 and its end at P'_4. The escape regions $E(O_1, -0)$ and $E(O_2, -0)$ are gray.

The arc of U'_2 from P_1 to the region $E(O_1, +0)$ has its image along the first arc of U'_3 that starts at the point P_2 and reaches the boundary of $E(O_1, -0)$ after infinite clockwise rotations. Similarly the arc of U'_2 from the region $E(O_1, +0)$ to the point P'_2 has its image on the third arc of U'_2 from the boundary of $E(O_1, -0)$ to the point P'_3 after infinite counterclockwise rotations.

If we continue the unstable asymptotic curve U, beyond the lobes U'_3 and U_3 in the case $h = 27$, we have a quite complicated lobe U'_4 (Figure 7). The curve U'_4 starts at P_3 with an arc making infinite clockwise rotations around $E(O_1, -0)$. A second branch (arc) starts by making infinite counterclockwise rotations around $E(O_1, -0)$. This arc does not terminate at a point Q, as in Figure 6, but passes below the lobe U'_1 of Figure 6, and makes infinite clockwise rotations around $E(O_2, -0)$ on the left part of Figure 7. Then a number of branches start asymptotically from the boundary of $E(O_2, -0)$ and return again asymptotically to it, both below the lobe U'_1 of Figure 6 and above this lobe. Finally, we have two more arcs, very close to the second and first arcs above. Namely, the branch before the last makes infinite counterclockwise rotations around $E(O_2, -0)$ and ends with infinite clockwise rotations around $E(O_1, -0)$ and the last branch starts with infinite counterclockwise rotations around $E(O_1, -0)$ and terminates at P'_4 very close to P_3 (Figure 7). Thus, although the lobe U'_1 of Figure 6 does not make infinite rotations around $E(O_2, -0)$ the lobe U'_3 makes infinite rotations around $E(O_1, -0)$ and the

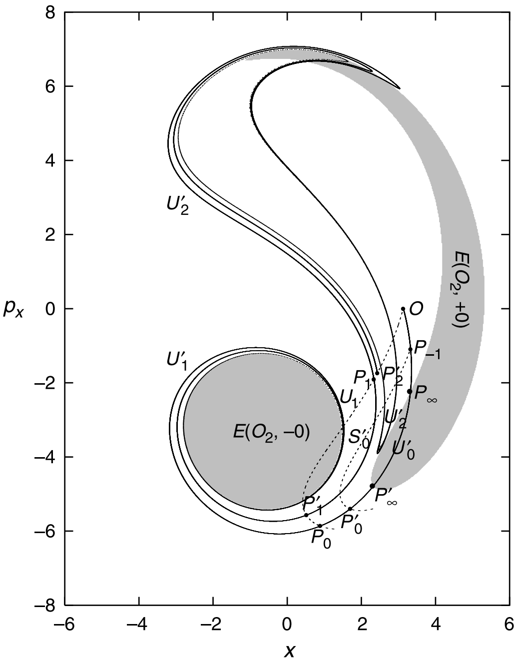

Figure 8. The lobes $U_0' \equiv S_0'$, U_1', U_1, U_2' and part of the lobe U_0 in the case $h = 29$. The escape regions $E(O_2, -0)$ and $E(O_2, +0)$ are gray.

higher lobe U_4' (Figure 7) makes infinite rotations around both $E(O_1, -0)$ and $E(O_2, -0)$.

For the energy $h = 27$ (Figure 6) the outer lobes U_1', U_2' are elongated but not of infinite length. On the other hand for $h = 29$ (Figure 8) the lobe U_1' makes infinite spiral rotations around $E(O_2, -0)$ and tends to a limiting asymptotic curve, which is the boundary of the region $E(O_2, -0)$. In fact U_1' is composed of two spiral curves. The first starts at P_0 and makes infinite rotations clockwise while the second makes infinite rotations counterclockwise and terminates at the point P_1' (Figure 8).The same is true with the lobes U_2', U_3', etc. As a consequence we cannot consider the curve U_1' as a unique curve, although its two arcs, the one starting at P_0 and the one ending at P_1', both approach asymptotically the same limiting curve. For $h = 27$ (Figure 6) the lobes U_1', U_2' are images of the lobe U_0' and they have equal area. This is due to the fact that no orbit starting in the area U_0' escapes after one or two iterations. On the other hand for $h = 29$ (Figure 8) the area of the lobe U_1' is smaller than the area of the lobe U_0' because some orbits from U_0' escape to infinity, before making another intersection with the plane (x, p_x). These are the orbits in the region which is common between $E(O_2, +0)$ and the lobe U_0'. Along the asymptotic curve U there are intervals that lead to escapes, as discussed in Contopoulos and Polymilis (1993). One such interval is the part $P_\infty P_\infty'$ of the arc U_0' inside the region $E(O_2, +0)$ (Figure 8).

The image of the arc $P_{-1}P_\infty$ of the asymptotic curve U is the first part of the boundary of the lobe U'_1, that starts at P_0 and terminates, after infinite clockwise rotations, on the boundary of $E(O_2, -0)$. This is explained in the same way as the spirals formed by $E(O_2, +1)$ around $E(O_1, +0)$ (Figure 2(a)) that we discussed above. The orbits along U between P_∞ and P'_∞ escape for positive times directly through the Lyapunov orbit O_2, without any further intersections with the plane (x, p_x). The orbit starting at P_∞ is on the stable manifold of O_2 and reaches O_2 after infinite time. The orbits between P_{-1} and P_∞ approach the orbit O_2 as t increases but they are reflected without reaching O_2, and then they continue close to the unstable manifold of O_2, reaching the plane (x, p_x) close to the boundary of $E(O_2, -0)$. If the initial point of an orbit approaches P_∞ its consequent approaches the boundary of $E(O_2, -0)$ being at the same time on the asymptotic curve U (beyond P_0) that approaches asymptotically this boundary. Thus, the images of the points of the arc $P_{-1}P_\infty$ follow the spiral from P_0 to the limiting curve (boundary of $E(O_2, -0)$) and approach asymptotically this boundary when the initial point tends to P_∞. The same happens with the arc $P'_\infty P'_0$ of the asymptotic curve U. Its image now is an arc starting on the boundary of $E(O_2, -0)$ and after infinite counterclockwise rotations around this boundary, it reaches the point P'_1.

The escape regions of the case $h = 27$ are smaller than the corresponding escape regions of the case $h = 29$, but they are similar in their form. As h decreases these escape regions become smaller and they disappear when h becomes smaller than h_{esc}. However, the structure of the asymptotic curves for h slightly smaller than h_{esc} resembles the form of these curves for $h > h_{\text{esc}}$. This is seen in Figure 9(a) and (b) for $h = 25.2 < h_{\text{esc}}$. In Figure 9(a) we see the outer lobes U'_1, U'_2, U'_3 and U'_4 that have a relatively small length and the lobe U'_5 that is longer. Higher order lobes are more complicated. In particular in Figure 9(b) we see the lobe U'_8 which is very complicated. Of course in Figure 9(b) we do not have infinite spiral rotations (infinite rotations appear only for $h > h_{\text{esc}}$), but nevertheless the lobe U'_8 makes some rotations in the regions that will form the escape regions $E(O_1, -0)$ and $E(O_2, -0)$ for a little larger h, namely when $h > h_{\text{esc}}$.

Two more unstable periodic orbits are of primary importance for the dynamics of the system, namely the Lyapunov orbits O_1 and O_2. The asymptotic curves of the orbit O_1 have been studied in detail in Contopoulos (1990a). In this case also we have escape regions that correspond to the escape regions described in the present paper.

The asymptotic manifolds of the orbits O_1 and O_2 intersect along homoclinic and heteroclinic orbits. In Figure 10(a) we give a homoclinic orbit reaching asymptotically the orbit O_1 for $t \to \pm\infty$ and in Figure 10(b) we give a heteroclinic orbit from O_1 reaching asymptotically the orbit O_2. Such orbits are important because they represent the limits between escaping and non-escaping orbits. Namely a small deviation from these orbits outwards, that is, an orbit crossing the orbit O_1, or O_2, escapes from the system to infinity, never returning close to the origin. On the other

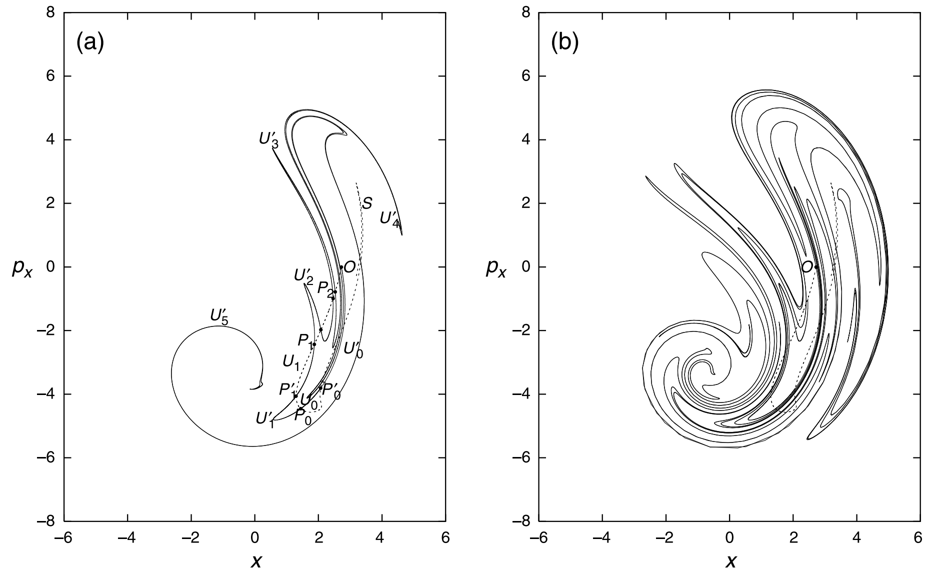

Figure 9. Some lobes in the case $h = 25.2$ ($< h_{esc} = 25.31$). (a) The lobes U'_0, U_0, U'_1, U_1, U'_2, U_2, U'_3, U_3, U'_4, U_4 and U'_5. (b) The lobe U_8 in the same case.

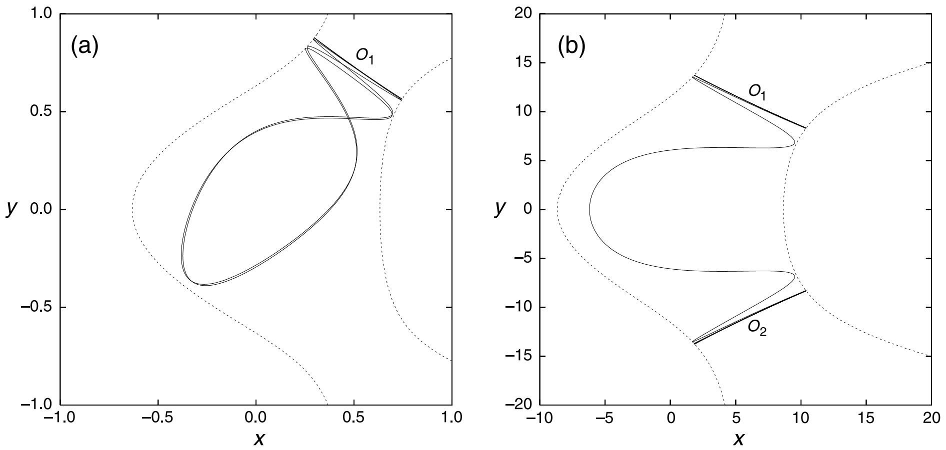

Figure 10. (a) A homoclinic orbit to the O_1 Lyapunov orbit. (b) A heteroclinic orbit between O_1 and O_2.

hand a small deviation of such an orbit inwards from the orbit O_1, or O_2, avoids the escape temporarily, but this orbit may escape later through one of the Lyapunov orbits.

5. Recurrence

In a previous paper (Contopoulos and Polymilis, 1993) we found the minimum Poincaré recurrence time for the lobes of the unstable orbit O. Namely we found the first higher order lobe U'_{k+1} that enters into the outer lobe U'_1 so that the two lobes partly overlap. We know that the unstable asymptotic curve cannot intersect itself, therefore the outer lobe U'_{k+1} must first enter into the resonance region, and intersect the lobe U'_1 from its inner side S'_1.

We found that for $h = 24$ the first outer lobe that enters into U'_1 is the lobe U'_{22}, therefore the minimum Poincaré recurrence time is $k = 21$.

In a similar way we found that for $h = 25$ the minimum recurrence time is $k = 15$. Furthermore, we noticed that although for $h > h_{\mathrm{esc}}$ the phase space is infinite and one cannot define an average Poincaré recurrence time (it is infinite), nevertheless, one can find a minimum Poincaré recurrence time. In particular for $h = 27$ the minimum recurrence time is $k = 6$ while for $h = 27.8$ it is $k = 5$.

In the present case we can see that for $h = 29$ the minimum recurrence time is $k = 2$. This can be derived from Figure 8 as follows. In this figure we have drawn the arc S'_0 of the stable asymptotic curve S that starts at the point P'_0 and ends at the point P_{-1}, forming the inner lobe $S'_0 \equiv U'_0$. Then we notice that the lobe U'_2 enters into the lobe U'_0. Therefore the lobe U'_3 enters into U'_1, and so on for higher order lobes. We verified that U'_3 enters into U'_1 by calculating U'_3 (U'_3 is very complicated and we do not give a figure of it).

The minimum recurrence time k as a function of the energy is given in Figure 11. As the energy increases the value of k decreases, until it reaches the value $k = 1$ for $h = 30$. Then it remains constant ($k = 1$), and it seems improbable that it can become smaller (this would require a large deformation of the lobe U'_1 to enter into itself).

The common region of U'_3 and U'_1 (recurrence region) for $h = 29$ is relatively small and does not approach the limiting curve of an escape region. However,

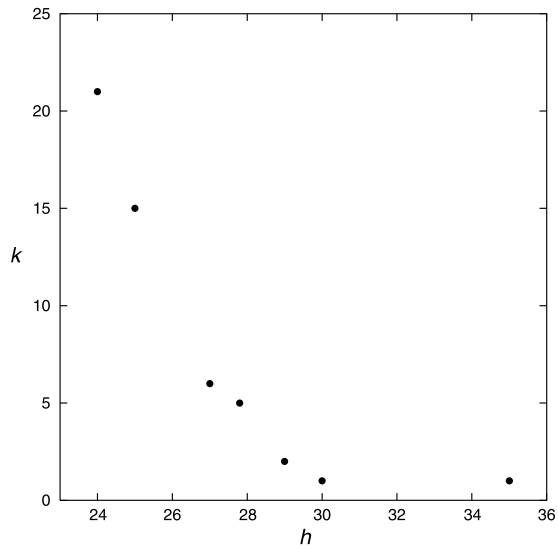

Figure 11. Minimum recurrence times for some values of the energy.

for larger h this region becomes larger and finally reaches asymptotically the escape region $E(O_2, -0)$ after infinite rotations. Thus its area is smaller than the corresponding common area between U_2' and U_0'.

For example in the case of $h = 29$ we have computed the area of $U_n' \cap U_{n+k}'$ (where $k = 2$ is the minimum recurrence time) beginning with $n = 0$. The lobe U_2' enters inside the lobe U_0' but also makes infinite rotations around $E(O_2, -1)$, (This escape region is shown in Figure 2(b) but not in Figure 8). Therefore, the intersection of U_2' and U_0' consists of a main area, shown in Figure 8, plus an infinite number of thin filaments. We considered only the main area, since the thin filaments are very small. Then we estimated the area of the images of the area $U_2' \cap U_0'$ by iterating a large number of randomly and homogeneously distributed initial conditions inside it and counting the number of orbits that remained after each iteration. The results are presented in Figure 12, where we can see that the ratio E_n/E_0 (where E_n denotes the area of the nth recurrence region) is reduced roughly exponentially although the slope of the diagram changes.

This reduction of the recurrence region as the order of the lobes increases is quite general. It is due to the fact that a part of the recurrence region escapes to infinity. As the order of the lobes increases further, the area of the recurrence region always decreases and tends to zero. This is to be expected because almost all the orbits that do not belong to islands of stability escape from the system.

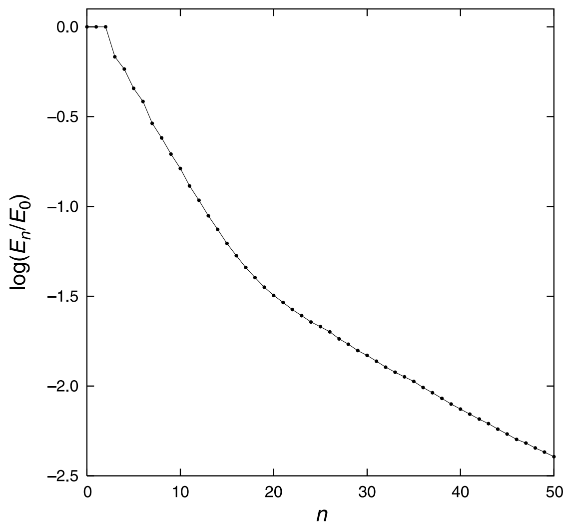

Figure 12. The ratio of the area E_n of the nth recurrence region to that of the initial recurrence region (E_0) as a function of n.

6. The Resonance 1:1

In this section we compare the behaviour of the Hamiltonian (1) with that of the Hamiltonian

$$H'(x, y, p_x, p_y) = \tfrac{1}{2}(p_x^2 + p_y^2 + x^2 + y^2) - xy^2 = h' \tag{5}$$

which is a perturbation of the 1:1 resonance. In this case the escape energy (given by (2)with $A = B = \epsilon = 1$) is $h'_{\mathrm{esc}} = 0.125$. A correspondence between the two cases can be established using the relation

$$\frac{h'}{h'_{\mathrm{esc}}} = \frac{h}{h_{\mathrm{esc}}}. \tag{6}$$

As the energy increases we have the following cases:

6.1. $h' = 0.13$

This corresponds roughly to the case $h = 27$ for the Hamiltonian (1). In Figure 13 we see that the two escape regions $E(O_i, +0)$, $i = 1, 2$ are almost symmetric with respect to the x-axis, in contrast with the 4:3 case (Figure 2(b)), where $E(O_2, +0)$ is roughly at the same position, but $E(O_1, +0)$ is very different from the corresponding region of the present case, being elongated along the right side of the phase space. Notice that now the y-axis orbit is unstable and there is a thin chaotic region near the boundary $x^2 + p_x^2 = 2h'$. Around the escape regions $E(O_i, +0)$ there are spiral regions $E(O_i, +1)$. The whole central domain of Figure 13 leads to escape after a short, or longer time n. The escape domain is surrounded by a

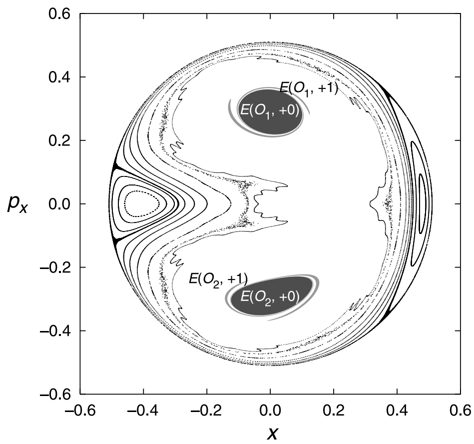

Figure 13. Escape regions in the Hamiltonian (5) for $h' = 0.13$. The dark gray regions represent the escape regions $E(O_{1,2}, +0)$. The light gray spiral regions represent the escape regions $E(O_{1,2}, +1)$.

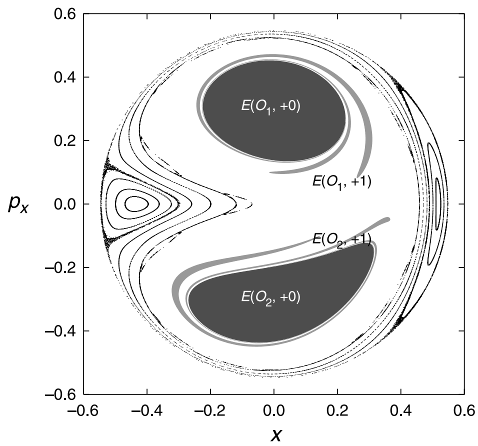

Figure 14. Escape regions in the Hamiltonian (5) for $h' = 0.15$. The dark gray regions represent the escape regions $E(O_{1,2}, +0)$. The light gray spiral regions represent the escape regions $E(O_{1,2}, +1)$.

strangely shaped invariant curve (a curve with many irregularities). Going from this invariant curve outwards towards the boundary we find a succession of zones containing invariant curves, and thin but not insignificant chaotic regions. Close to the boundary, on the left and on the right, there are two large islands of stability. This structure is quite different than that of the system (1), where there is a zone composed mostly of invariant curves (Figure 2(b)) without any visible chaotic regions, extending up to the boundary, that is, the stable *y*-axis orbit.

6.2. $h' = 0.15$

In Figure 14 we see that the main escape regions $E(O_i, +0)$, $E(O_i, +1)$ have grown considerably in size. The total escape domain has also been extended outwards, by the destruction of some invariant curves, in particular the irregularly shaped invariant curves that exist for $h' = 0.13$. In their place there are now cantori. Although these cantori can be crossed by the orbits, they also serve as partial barriers that confine escaping orbits for long times before these orbits can escape.

6.3. $h' = 0.18$

This case corresponds roughly to the case $h = 40$ of the Hamiltonian (1). In Figure 15 we see that the asymmetry between the two principal escape regions $E(O_i, +0)$ is now much more pronounced. These two regions have grown considerably in size and they occupy now most of the phase space. Notice also that the escape region $E(O_2, +1)$ is now making infinite rotations around both principal escape regions $E(O_i, +0)$. All the invariant curves, that separated the escape domain from the boundary in Figures 13 and 14, have been destroyed. This is in contrast with the $h = 40$ case in the Hamiltonian (1) where there are still invariant curves

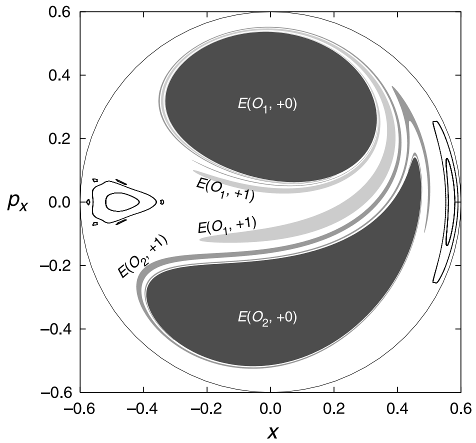

Figure 15. The escape regions in the Hamiltonian (5) for $h' = 0.18$. The dark gray regions represent the escape regions $E(O_{1,2}, +0)$. The medium gray regions represent the escape region $E(O_2, +1)$, and the light gray regions represent the escape regions $E(O_1, +1)$. Some islands of stability appear near the left and right boundary but detached from it.

near the boundary. The only prominent non-escaping orbits in the case $h' = 0.18$ are the two islands at the left and the right of Figure 15.

The escape rates for the Hamiltonian (5) are similar to the corresponding rates for the Hamiltonian (1). In Figure 16 we have plotted $dN_n/(N_0 - N_{\text{non}})$ as a function of the number of iterations n and we see the same qualitative behaviour as in Figure 5(a).

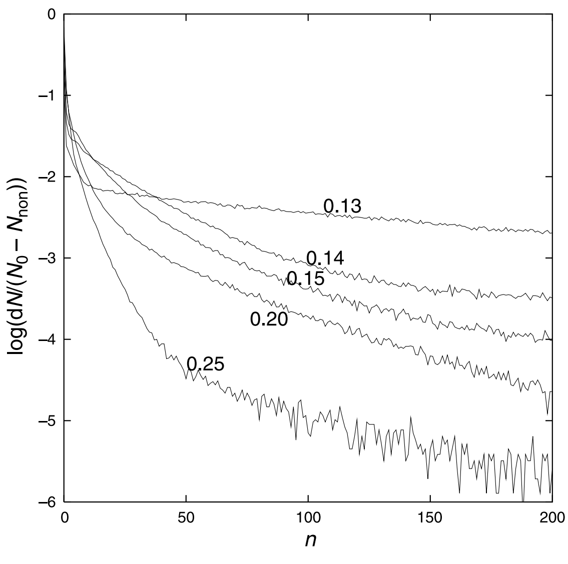

Figure 16. The escape rates in the Hamiltonian (5) for the energies $h' = 0.13$, $h' = 0.14$, $h' = 0.15$, $h' = 0.20$ and $h' = 0.25$, as functions of n.

7. Conclusions

An autonomous Hamiltonian system with escapes, although it is conservative, has an attractor at infinity. Thus, in some respects, it is similar to a dissipative system. In particular although the volumes in phase space are preserved, the areas on the plane (x, p_x) are not preserved. Thus, the plane (x, p_x), which is a Poincaré surface of section when the energy is smaller than the escape energy h_{esc}, is not a Poincaré surface of section for $h > h_{\text{esc}}$, except in a local sense (Birkhoff, 1927).

The domains of escape are reduced in size (i.e. in area) as the number of intersections increases. Most of the escape regions form infinite rotations around the main escape regions. The higher order escape regions form fractals. For example, close to the escape regions $E(O_i, \pm 1)$, $i = 1, 2$ there are infinite filaments of type $E(O_i, \pm n)$.

The asymptotic curves of the main unstable periodic orbits form complicated structures. In the present paper we study mainly the asymptotic curves of the central periodic orbit. These curves form outer lobes that become longer as the order increases. The higher order lobes develop infinite spirals around the escape regions $E(O_i, \pm 0)$. Thus, beyond a certain order the lobes have infinite length and reach asymptotically the boundaries of the escape regions. The areas of these lobes become smaller as the order increases.

In a system with escapes one cannot define an average Poincaré recurrence time. However, there is a minimum recurrence time for certain regions of the plane (x, p_x). In particular we studied the time required for an image of a particular lobe to intersect the same lobe. For large energies this time is very small. The domains of recurrence after some iterations become infinitely elongated, like the corresponding lobes. This implies that the higher order recurrence domains become smaller in area. Their area tends to zero as the number of iterations tends to infinity.

Finally, we studied the case of a Hamiltonian in 1:1 resonance (5). A major difference between this case and the case of the Hamiltonian (1), which is in a 4:3 resonance, is that in the 4:3 case the escape regions extend outwards but they do not reach the y-axis orbit (boundary), which is surrounded by invariant curves even for comparatively high energies ($h = 40$). On the other hand, in the case of the 1:1 resonance, the y-axis orbit is unstable and a chaotic region is formed around it, that is, near the boundary. As the energy increases the central escape domain grows and extends towards the boundary by the successive destruction of rings of invariant curves. Each such ring separates some small chaotic regions from the large escape domain. When such a ring is destroyed a chaotic region becomes connected with the large escape domain, therefore orbits that start in the chaotic region can now escape, but after a long time. Finally, the escape domain reaches the boundary for $h' \simeq 0.18$ (corresponding roughly to $h = 40$ in the Hamiltonian (1)) and then the only non-escaping orbits either belong to isolated islands inside the escape domain or they are intersections of the stable and unstable manifolds of unstable periodic orbits.

The resonance effects of a particular higher order resonance extend over a small interval of frequencies $|\omega_1{:}\omega_2 - n{:}m| = O(\epsilon^2)$ and they refer to initial conditions in an area of order $O(\epsilon^{(m+n-4)/2})$ (Contopoulos, 2002; pp. 107, 189). This area is very small if $m+n$ is large, and it is appreciable only if $m+n$ is small (e.g. $m=n=2$). Therefore we expect that the qualitative aspects of our results for the case $n{:}m = 4{:}3$ regarding the form of the asymptotic curves, the laws for the rate of escapes and the recurrence are also valid for most non-resonant Hamiltonians. Only in low order resonances, like the case 1:1, there are some important differences.

Acknowledgements

This research was supported by the Research Committee of the Academy of Athens.

References

Benet, L., Trautman, D. and Seligman, T.: 1997, 'Chaotic scattering in the restricted three-body problem. I. The Copenhagen problem', *Celest. Mech. & Dyn. Astr.* **66**, 203–228.

Benet, L., Seligman, T. and Trautman, D.: 1998, 'Chaotic scattering in the restricted three-body problem. II. Small mass parameters', *Celest. Mech. & Dyn. Astr.* **71**, 167–189.

Birkhoff, G.: 1927, *Dynamical Systems*, AMS, Providence, RI.

Bleher, S., Grebogi, C., Ott, E. and Brown, R.: 1988, 'Fractal boundaries for exit in Hamiltonian dynamics', *Phys. Rev. A* **38**, 930–938.

Churchill, R., Pecelli, G. and Rod, D.: 1975, 'Isolated unstable periodic orbits', *J. Diff. Eqn.* **17**, 329–348.

Contopoulos, G.: 1990a, 'Asymptotic curves and escapes in Hamiltonian systems', *Astron. Astrophys.* **231**, 41–55.

Contopoulos, G.: 1990b, 'Periodic orbits and chaos around two black holes', *Proc. Roy. Soc. London A* **431**, 183–202.

Contopoulos, G.: 1991, 'Periodic orbits and chaos around two fixed black holes. II', *Proc. Roy. Soc. London A* **435**, 551–562.

Contopoulos, G.: 2002, *Order and Chaos in Dynamical Astronomy*, Astronomy and Astrophysics Library, Springer, Berlin.

Contopoulos, G. and Kaufmann, D.: 1992, 'Types of escapes in a simple Hamiltonian system', *Astron. Astrophys.* **253**, 379–388.

Contopoulos, G. and Polymilis, C.: 1993, 'Geometrical and dynamical properties of homoclinic tangles in a simple Hamiltonian system', *Phys. Rev. E* **47**, 1546–1557.

Eckhardt, B.: 1988, 'Irregular scattering', *Physica D* **33**, 89–98.

Hénon, M.: 1989, 'La diffusion chaotique', *La Recherche* **209**, 490–498.

Henrard, J. and Navarro, J.F.: 2001, 'Spiral structures and chaotic scattering of coorbital satellites', *Celest. Mech. & Dyn. Astr.* **79**, 297–314.

Jung, C. and Scholz, H.: 1988, 'Chaotic scattering off the magnetic dipole', *J. Phys. A* **21**, 2301–2311.

Kandrup, H., Siopis, C., Contopoulos, G. and Dvorak, R.: 1999, 'Diffusion and scaling in escapes from two-degrees-of-freedom Hamiltonian systems', *Chaos* **9**, 381–392.

Ott, E. and Tél, T.: 1993, 'Chaotic scattering: An introduction', *Chaos* **3**, 417–426.

Petit, J.M. and Hénon, M.: 1986, 'Satellite encounters', *Icarus* **66**, 536–555.

Siopis, C., Kandrup, H.E., Contopoulos, G. and Dvorak, R.: 1997, 'Universal properties of escape in dynamical systems', *Celest. Mech. & Dyn. Astr.* **65**, 57–68.